Latin American Journal of Mathematics
Vol. 5, No. 1, 2026, pp. 69–87
10.14244/lajm.v5i1.111
ISSN: 2965-0798
www.lajm.ufscar.br

A fast adjoint-free shape gradient for p-Laplacian compliance: algorithmic speedup and engineering benchmarks

Yasser Yousfi [1]

[1] *Department of Mathematics, Faculty of Sciences, University Mohammed I, Oujda, Morocco*

E-mails: yousfi.98@gmail.com

Received: 25 May 2026 • **Accepted:** 31 July 2026 • **Published:** 10 August 2026

Abstract

Shape optimization of nonlinear membranes and non-Newtonian flow domains governed by the p-Laplace operator is hampered by the cost of an auxiliary linearised adjoint solve at every iteration. We show that this solve is unnecessary: a self-adjoint identity reduces the adjoint state to a multiple of the primal state, halving the PDE cost per iteration. We derive a closed-form boundary expression of the shape gradient, extend the analysis to the singular regime $1 < p < 2$ via Muckenhoupt-weighted Sobolev spaces, and prove subsequential convergence of the resulting descent algorithm. Three engineering benchmarks (cantilever, MBB beam, short bridge) for $p \in \{1.5, 2, 3, 4\}$ deliver compliance reductions of up to 51.8%, demonstrate a CPU speedup of up to 25% over the classical full-adjoint method, and confirm identical iterates to floating-point precision. The framework integrates readily into existing finite-element shape-optimization codes.

Keywords: shape optimization, p-Laplacian, compliance minimization, adjoint-free method, nonlinear elasticity, benchmark problems

MSC2020: 49Q10, 35J92, 49Q12, 49M41, 65N30

1 Introduction

Shape optimization concerns finding a domain $\Omega \subset \mathbb{R}^N$ that minimizes a cost functional under PDE constraints. Following the seminal work of Hadamard [14], the field has been developed systematically since the 1970's [1, 16, 20, 22, 23].

We consider the geometric optimization of a nonlinear membrane modelled by the p-Laplace operator $\Delta_p u := \operatorname{div}(|\nabla u|^{p-2}\nabla u)$, $1 < p < \infty$. Such operators arise in nonlinear diffusion, non-Newtonian fluid mechanics, glaciology, image processing, and membranes with nonlinear constitutive laws. We minimize the compliance under a fixed volume constraint, the prototypical shape-optimization problem.

Computational bottleneck. Existing approaches based on Hadamard boundary perturbation [1, 16, 25] yield a *volume expression* of the shape gradient that requires solving an additional linearised adjoint problem at every iteration. For $p \neq 2$, this adjoint has a degenerate weight $|\nabla u|^{p-2}$, is delicate to discretise, and adds 25–50% to the per-iteration cost (Section 8.7).

Recent context. Recent advances address level-set mesh evolution [2, 7], $W^{1,\infty}/p$-harmonic descent directions [8, 19, 24], convergence analyses [9], null-space gradient flows [12], and preconditioned descent algorithms for p-Laplacian variational problems [13]. The cost of the $p \neq 2$ adjoint solve has received little attention.

Contributions of this work

(C1) **An adjoint-free shape gradient formula (Theorem 5.2).** We exploit a self-adjoint identity (Section 4) to derive a closed-form boundary expression

$$J'(\Omega)(\theta) = \frac{1}{p-1}\int_\Gamma \left(p\, f u - |\nabla u|^p\right) \theta \cdot n \, ds, \tag{1.1}$$

involving *only the primal state u and the data*. No linearised adjoint is solved. The identity recovers the Allaire formula [1, Ch. 6] as $p \to 2$.

(C2) **Weighted Sobolev framework for the singular regime (Proposition 4.5).** For $p \geq 2$ the analysis takes place in the standard Sobolev space. For $1 < p < 2$ the natural setting is the Muckenhoupt-weighted Sobolev space $H^1_\omega(\Omega; \Gamma_D)$ with $\omega = |\nabla u|^{p-2} \in A_2(\Omega)$; the self-adjoint identity carries over by density. This extends the analysis [25] to a regime where the classical adjoint approach is delicate.

(C3) **Engineering benchmarks and quantified speedup (Sections 7–8).** Three benchmarks (cantilever, MBB, bridge) for $p \in \{1.5, 2, 3, 4\}$ deliver compliance reductions up to 51.8%. A head-to-head CPU comparison (Section 8.7) confirms identical iterates to floating-point precision and a CPU speedup of 3–25%. A finite-difference test verifies the formula; a mesh-refinement study gives a measured rate ≈ 3.6. Subsequential convergence is proved (Theorem 7.2).

(C1) reduces the adjoint to the trivial identity $q = u/(p-1)$, so the gradient depends only on the primal state. The framework integrates as a one-line replacement in any existing shape-optimization code; FreeFem++ and Python implementations are provided as supplementary material.

Outline

Sections 2–3 fix notation and well-posedness. Section 4 proves the self-adjoint identity and the weighted Sobolev framework (Proposition 4.5). Section 5 derives the boundary gradient. Section 6 addresses existence; Section 7 describes the algorithm and proves convergence; Section 8 reports the experiments.

2 Preliminaries

2.1 Functional spaces and the p-Laplacian

Throughout the paper, Ω denotes a bounded open subset of $\mathbb{R}^N$ ($N \geq 2$) with Lipschitz boundary $\partial\Omega$. We assume that $\partial\Omega$ is partitioned into three pairwise disjoint relatively open parts of positive $(N-1)$-dimensional Hausdorff measure:

$$\partial\Omega = \overline{\Gamma} \cup \overline{\Gamma_N} \cup \overline{\Gamma_D}, \tag{2.1}$$

where Γ_D carries homogeneous Dirichlet (clamped) boundary conditions, Γ_N carries inhomogeneous Neumann (loaded) boundary conditions, and Γ is the *free* part of the boundary on which the optimization acts.

For $1 < p < \infty$, $W^{1,p}(\Omega)$ denotes the standard Sobolev space, and we introduce the closed subspace

$$V(\Omega) \;:=\; \left\{ v \in W^{1,p}(\Omega) \;:\; v = 0 \text{ on } \Gamma_D \right\}, \tag{2.2}$$

endowed with the norm $\|\nabla v\|_{L^p(\Omega)}$ which is equivalent to the full $W^{1,p}$-norm by virtue of the Poincaré inequality and the assumption $\mathrm{meas}_{N-1}(\Gamma_D) > 0$.

The p-Laplace operator is defined formally by

$$\Delta_p u \;:=\; \mathrm{div}\big(|\nabla u|^{p-2}\nabla u\big). \tag{2.3}$$

For $p = 2$, $\Delta_p = \Delta$ is the linear Laplacian. For $p \neq 2$, Δ_p is a quasilinear, monotone operator (degenerate elliptic if $p > 2$, singular if $p < 2$); see [17] for a comprehensive treatment.

2.2 Admissible shapes

Following [1, 20, 25], we consider perturbations of a reference domain Ω_0 by Lipschitz diffeomorphisms close to the identity. Let $\mathcal{T} := \{T : \mathbb{R}^N \to \mathbb{R}^N : T - \mathrm{Id}, T^{-1} - \mathrm{Id} \in W^{1,\infty}\}$ and $\mathcal{C}(\Omega_0) := \{T(\Omega_0) : T \in \mathcal{T}\}$, equipped with the pseudo-distance

$$d(\Omega_1, \Omega_2) := \inf\big\{\|T - \mathrm{Id}\|_{W^{1,\infty}} + \|T^{-1} - \mathrm{Id}\|_{W^{1,\infty}} \;:\; T \in \mathcal{T},\ T(\Omega_1) = \Omega_2\big\}. \tag{2.4}$$

We keep $\Gamma_D \cup \Gamma_N$ fixed and write $\Theta_{\mathrm{ad}} := \{\theta \in W^{1,\infty}(\mathbb{R}^N, \mathbb{R}^N) : \theta = 0 \text{ near } \overline{\Gamma_D} \cup \overline{\Gamma_N}\}$. For $\theta \in \Theta_{\mathrm{ad}}$ with $\|\theta\|_{W^{1,\infty}} < 1$, the map $T = \mathrm{Id} + \theta$ is a bi-Lipschitz homeomorphism in $\mathcal{T}$ [1, 20], and we set $\Omega_\theta := (\mathrm{Id} + \theta)(\Omega_0)$.

2.3 Differentiability with respect to the domain

A functional $J : \mathcal{C}(\Omega_0) \to \mathbb{R}$ is *shape differentiable at* Ω_0 if $\theta \mapsto J((\mathrm{Id} + \theta)(\Omega_0))$ is Fréchet differentiable at 0 in $W^{1,\infty}(\mathbb{R}^N, \mathbb{R}^N)$, with derivative $J'(\Omega_0)$. The Hadamard structure theorem [16, 23] states that $J'(\Omega_0)(\theta)$ depends only on $\theta \cdot n$ on $\partial\Omega_0$. The standard change-of-variable lemmas below are from [16, Ch. 5] or [1, Ch. 6].

Lemma 2.1 (Change of variables). *Let $T \in \mathcal{T}$ and $\Omega_0 \subset \mathbb{R}^N$ open. For $1 \leq p \leq \infty$,*

(i) $f \in L^p(T(\Omega_0)) \iff f \circ T \in L^p(\Omega_0)$, *with* $\displaystyle\int_{T(\Omega_0)} f\,dx = \int_{\Omega_0} (f \circ T)\,|\det \nabla T|\,dy;$

(ii) $f \in W^{1,p}(T(\Omega_0)) \iff f \circ T \in W^{1,p}(\Omega_0)$, *with* $(\nabla f) \circ T = (\nabla T)^{-\top}\nabla(f \circ T);$

(iii) if T is of class C^1 then for $f \in L^p(\partial T(\Omega_0))$, $\displaystyle\int_{\partial T(\Omega_0)} f\,dS = \int_{\partial\Omega_0} (f \circ T)\,|\det \nabla T|\,\big|(\nabla T)^{-\top} n\big|\,dS.$

Lemma 2.2 (Differentiation of volume integrals [16, Prop. 5.4.18]). *Let Ω_0 be a bounded open set with Lipschitz boundary, $f \in W^{1,1}(\mathbb{R}^N)$, and $J(\Omega) := \int_\Omega f\,dx$. Then J is shape differentiable at Ω_0 and*

$$J'(\Omega_0)(\theta) \;=\; \int_{\partial\Omega_0} f\,\theta \cdot n\,ds, \qquad \theta \in W^{1,\infty}(\mathbb{R}^N, \mathbb{R}^N).$$

Lemma 2.3 (Differentiation of surface integrals [16, Prop. 5.4.18]). *Let Ω_0 be of class C^2, $f \in W^{2,1}(\mathbb{R}^N)$, and $J(\Omega) := \int_{\partial\Omega} f\,ds$. Then J is shape differentiable at Ω_0 and*

$$J'(\Omega_0)(\theta) \;=\; \int_{\partial\Omega_0} (\nabla f \cdot n + Hf)\,\theta \cdot n\,ds \;=\; \int_{\partial\Omega_0} \Big(\partial_n f + Hf\Big)\theta \cdot n\,ds,$$

where $H = \mathrm{div}\, n$ is the mean curvature of $\partial\Omega_0$.

3 State problem and the compliance functional

3.1 The state equation

Given $\Omega \in \mathcal{C}(\Omega_0)$, $f \in W^{1,p}(\mathbb{R}^N)$ and $g \in W^{2,p}(\mathbb{R}^N)$, we look for $u \in V(\Omega)$ such that

$$\begin{cases} -\Delta_p u = f & \text{in } \Omega, \\ u = 0 & \text{on } \Gamma_D, \\ |\nabla u|^{p-2}\partial_n u = g & \text{on } \Gamma_N, \\ |\nabla u|^{p-2}\partial_n u = 0 & \text{on } \Gamma. \end{cases} \tag{3.1}$$

The variational formulation reads: find $u \in V(\Omega)$ such that

$$\int_\Omega |\nabla u|^{p-2}\nabla u \cdot \nabla v \, dx = \int_\Omega f\, v \, dx + \int_{\Gamma_N} g\, v \, ds, \qquad \forall v \in V(\Omega). \tag{3.2}$$

Proposition 3.1 (Well-posedness of the state)**.** *Under the standing assumptions, problem* (3.2) *admits a unique solution $u \in V(\Omega)$. Moreover, there exists $C = C(p, \Omega, \Gamma_D) > 0$ such that*

$$\|u\|_{W^{1,p}(\Omega)} \;\le\; C\Big(\|f\|_{L^{p'}(\Omega)}^{1/(p-1)} + \|g\|_{L^{p'}(\Gamma_N)}^{1/(p-1)}\Big), \qquad p' := \frac{p}{p-1}.$$

Proof. The operator $\mathcal{A}u := -\Delta_p u$ is monotone, continuous, and coercive on $V(\Omega)$; the Browder–Minty theorem [26, Ch. 26] yields existence and uniqueness, and the estimate follows from coercivity. □

3.2 Energy formulation and the compliance

The state u is also the unique minimizer in $V(\Omega)$ of the energy

$$\mathcal{E}(\Omega; v) \;:=\; \frac{1}{p}\int_\Omega |\nabla v|^p \, dx - \int_\Omega f\, v\, dx - \int_{\Gamma_N} g\, v \, ds. \tag{3.3}$$

Definition 3.2 (Compliance)**.** *The compliance functional is*

$$J(\Omega) \;:=\; \int_\Omega f\, u\, dx + \int_{\Gamma_N} g\, u\, ds, \tag{3.4}$$

where $u \in V(\Omega)$ is the unique solution of (3.2).

The following identity will be crucial.

Lemma 3.3 (Energy identity)**.** *Let u solve* (3.2)*. Then*

$$J(\Omega) \;=\; \int_\Omega |\nabla u|^p \, dx, \qquad \textit{equivalently} \qquad \mathcal{E}(\Omega; u) \;=\; -\frac{p-1}{p} J(\Omega). \tag{3.5}$$

Proof. Take $v = u$ in (3.2): $\int_\Omega |\nabla u|^p \, dx = \int_\Omega f u \, dx + \int_{\Gamma_N} g u \, ds = J(\Omega)$. □

The shape optimization problem under consideration is

$$\inf_{\Omega \in \mathcal{U}_{\mathrm{ad}}^R} J(\Omega), \qquad \mathcal{U}_{\mathrm{ad}}^R := \big\{\Omega \in \mathcal{C}(\Omega_0) : \; d(\Omega, \Omega_0) \le R, \; \Gamma_D \cup \Gamma_N \subset \partial\Omega, \; |\Omega| = V_0\big\}, \tag{3.6}$$

where V_0 is a prescribed volume.

4 Self-adjoint structure of the p-Laplacian compliance

This section establishes the central algebraic identity of the paper: the adjoint state associated with the compliance functional admits the simple closed form $q = u/(p-1)$ for every $1 < p < \infty$. The functional analysis underlying this identity has two distinct regimes:

- For *super-quadratic* $p \geq 2$, the analysis takes place in the standard Sobolev space $V(\Omega)$ and the adjoint equation is handled by the classical Lax–Milgram lemma (Section 4.1–4.2).
- For *sub-quadratic* $1 < p < 2$, the linearised adjoint operator becomes singular at the critical set $\{\nabla u = 0\}$ and the natural functional setting is the *Muckenhoupt-weighted Sobolev space* $H^1_\omega(\Omega; \Gamma_D)$ with $\omega = |\nabla u|^{p-2} \in A_2(\Omega)$. This case is treated in Section 4.3 (Proposition 4.5) and constitutes one of the main theoretical contributions of the paper.

4.1 The Lagrangian and the adjoint problem

We introduce the Lagrangian

$$\mathcal{L}(\Omega, v, q) \; := \; \underbrace{\int_\Omega f\, v\, dx + \int_{\Gamma_N} g\, v\, ds}_{=J(\Omega;v)} \; - \; \underbrace{\left[\int_\Omega |\nabla v|^{p-2}\nabla v \cdot \nabla q\, dx - \int_\Omega f\, q\, dx - \int_{\Gamma_N} g\, q\, ds\right]}_{\text{constraint}}, \tag{4.1}$$

defined for $v, q \in V(\Omega)$. Whenever v solves the state equation (3.2), the bracketed term vanishes for every $q \in V(\Omega)$, hence $\mathcal{L}(\Omega, u, q) = J(\Omega)$ identically in q.

The first-order optimality condition for the Lagrangian gives:

- $\partial_q \mathcal{L}(\Omega, v, q) \cdot \tilde{q} = 0$ for all $\tilde{q} \in V(\Omega)$ recovers the state equation (3.2);
- $\partial_v \mathcal{L}(\Omega, v, q) \cdot \tilde{v} = 0$ for all $\tilde{v} \in V(\Omega)$ defines the adjoint problem.

Lemma 4.1 (Linearization of the p-Laplacian). *The Fréchet derivative of the map $V(\Omega) \longrightarrow L^{p'}(\Omega; \mathbb{R}^N)$, $v \mapsto |\nabla v|^{p-2}\nabla v$, at $u \in V(\Omega)$ in direction $\tilde{v} \in V(\Omega)$ is*

$$D\big(|\nabla u|^{p-2}\nabla u\big)(\tilde{v}) \; = \; |\nabla u|^{p-2}\nabla\tilde{v} + (p-2)|\nabla u|^{p-4}(\nabla u \cdot \nabla \tilde{v})\, \nabla u, \tag{4.2}$$

in a pointwise almost everywhere sense, valid where $\nabla u \neq 0$ (and trivially extended otherwise when $p \geq 2$).

Proof. Set $\Phi(\xi) := |\xi|^{p-2}\xi$ for $\xi \in \mathbb{R}^N$. A direct computation gives, for $\xi \neq 0$,

$$D\Phi(\xi)\eta = |\xi|^{p-2}\eta + (p-2)|\xi|^{p-4}(\xi \cdot \eta)\xi,$$

which yields (4.2) by the chain rule. The integrability assertion follows from $|D\Phi(\xi)| \leq (p-1)|\xi|^{p-2}$ and Hölder's inequality. □

Imposing $\partial_v \mathcal{L}(\Omega, u, q) \cdot \tilde{v} = 0$ and using Lemma 4.1, we obtain the *linearized adjoint equation*: find $q \in V(\Omega)$ such that for every $\tilde{v} \in V(\Omega)$,

$$\int_\Omega \Big[|\nabla u|^{p-2}\nabla q + (p-2)|\nabla u|^{p-4}(\nabla u \cdot \nabla q)\, \nabla u\Big] \cdot \nabla\tilde{v}\, dx \; = \; \int_\Omega f\, \tilde{v}\, dx + \int_{\Gamma_N} g\, \tilde{v}\, ds, \tag{4.3}$$

where $B_u(q, \tilde{v})$ denotes the bilinear form on the left-hand side of (4.3).

Remark 4.2. *B_u is manifestly symmetric in $(q, \tilde{v})$, reflecting the fact that the compliance is the value of a self-dual problem.*

4.2 Identity in the standard regime ($p \geq 2$)

The following result is the cornerstone of our analysis.

Theorem 4.3 (Self-adjoint structure). *Let $u \in V(\Omega)$ be the unique solution of (3.2) and assume the linearized adjoint equation (4.3) admits a unique solution $q \in V(\Omega)$. Then*

$$\boxed{q \;=\; \frac{u}{p-1}} \tag{4.4}$$

holds in $V(\Omega)$. Equivalently, the adjoint state is collinear to the state, with proportionality constant $1/(p-1)$.

Proof. Set $\hat{q} := u/(p-1)$. Substituting in the left-hand side of (4.3) and collecting the $|\nabla u|^{p-2}$ terms,

$$\int_\Omega |\nabla u|^{p-2}\nabla u \cdot \nabla \tilde{v}\, \frac{1+(p-2)}{p-1}\, dx = \int_\Omega |\nabla u|^{p-2}\nabla u \cdot \nabla \tilde{v}\, dx,$$

which by (3.2) equals $\int_\Omega f\tilde{v}\, dx + \int_{\Gamma_N} g\tilde{v}\, ds$, the right-hand side of (4.3). Uniqueness yields $q = \hat{q}$. □

Remark 4.4 (Strong form and uniqueness). *Integration by parts of (4.3) yields the natural boundary conditions $|\nabla u|^{p-2}\partial_n q = 0$ on Γ, $q = 0$ on Γ_D, and the linearised Neumann condition on Γ_N. For $p \geq 2$, B_u is continuous and coercive on $\{q \in V(\Omega) : |\nabla u|^{(p-2)/2}\nabla q \in L^2(\Omega)\}$ and Lax–Milgram applies; Theorem 4.3* constructs *the unique adjoint state.*

4.3 Singular regime ($1 < p < 2$): weighted Sobolev framework

For $1 < p < 2$, Δ_p becomes *singular* at $\{\nabla u = 0\}$ and the Lax–Milgram argument requires Muckenhoupt-weighted Sobolev spaces [6, 11]. Fix $u \in V(\Omega)$ solving (3.2) and set $\omega(x) := |\nabla u(x)|^{p-2}$ (singular on $\{\nabla u = 0\}$). The natural energy space is

$$H^1_\omega(\Omega;\Gamma_D) \;:=\; \left\{ q \in W^{1,1}_{\mathrm{loc}}(\Omega) \;:\; \int_\Omega \omega\, |\nabla q|^2\, dx < \infty,\;\; q = 0 \text{ on } \Gamma_D \right\}, \tag{4.5}$$

endowed with the inner product $\langle q, v\rangle_\omega := \int_\Omega \omega\, \nabla q \cdot \nabla v\, dx$. A sufficient condition for $H^1_\omega(\Omega;\Gamma_D)$ to be a Hilbert space, for $C_c^\infty(\Omega \setminus \overline{\Gamma_D})$ to be dense in it, and for a weighted Poincaré inequality to hold, is that $\omega \in A_2(\Omega)$ *i.e.* ω belongs to the Muckenhoupt class:

$$\sup_{B\subset\Omega} \frac{1}{|B|}\int_B \omega\, dx \cdot \frac{1}{|B|}\int_B \omega^{-1}\, dx \;<\; +\infty, \tag{4.6}$$

over all balls in Ω. For $1 < p < 2$, $\omega = |\nabla u|^{p-2} \in A_2(\Omega)$ provided $|\nabla u| \in A_{2/(2-p)}(\Omega)$; this holds when $u \in W^{1,r}(\Omega)$ for $r > 2/(2-p)$ and ∇u does not concentrate on a null set [6, Th. 9].

Proposition 4.5 (Adjoint problem, sub-quadratic case). *Let $1 < p < 2$, $u \in V(\Omega)$ solve (3.2), and assume $\omega := |\nabla u|^{p-2} \in A_2(\Omega)$. Then the bilinear form B_u of (4.3) is continuous and coercive on $H^1_\omega(\Omega;\Gamma_D) \times H^1_\omega(\Omega;\Gamma_D)$, and the linearized adjoint problem admits a unique solution $q \in H^1_\omega(\Omega;\Gamma_D)$. The identity $q = u/(p-1)$ remains valid, since $u \in H^1_\omega(\Omega;\Gamma_D)$ as well by virtue of the energy identity $\int_\Omega |\nabla u|^p\, dx < \infty$, which can be rewritten as $\int_\Omega \omega\, |\nabla u|^2\, dx < \infty$.*

Proof. For $q, \tilde{v} \in H^1_\omega(\Omega;\Gamma_D)$, by Hölder's inequality with weights,

$$|B_u(q,\tilde{v})| \leq (p-1)\int_\Omega |\nabla u|^{p-2}|\nabla q||\nabla \tilde{v}| \leq (p-1)\, \|q\|_\omega\, \|\tilde{v}\|_\omega,$$

and coercivity follows from $B_u(q,q) \geq \int_\Omega |\nabla u|^{p-2}|\nabla q|^2\,dx = \|q\|_\omega^2$. The Lax–Milgram lemma in the Hilbert space $H^1_\omega(\Omega;\Gamma_D)$ provides existence and uniqueness. The identity $q = u/(p-1)$ verified in Theorem 4.3 carries over verbatim, since both sides of the variational equation are continuous on $H^1_\omega(\Omega;\Gamma_D)$ and agree on the dense subset $C_c^\infty(\Omega \setminus \overline{\Gamma_D})$. □

Remark 4.6 (Regularity assumption). *The assumption $\omega \in A_2(\Omega)$ rules out gradient vanishing on a large set. For nondegenerate p-Laplacian problems with regular data ($f, g \in C^{0,\alpha}$), Tolksdorf–Lieberman–DiBenedetto regularity [10, 17] gives $u \in C^{1,\beta}_{\mathrm{loc}}$ and the critical set has locally finite $(N-1)$-Hausdorff measure; in $N = 2$, $\omega \in A_2$ holds generically. At the discrete level, we add $\varepsilon = 10^{-12}$ to $|\nabla u|^2$ to sidestep this issue.*

5 Shape derivative of the compliance

5.1 Differentiability of the state map

The first step is to ensure that the parametrized state $u(\Omega_\theta)$ is sufficiently regular as a function of θ in a neighbourhood of 0.

Proposition 5.1 (Differentiability of the state, [1, 25]). *Assume Ω_0 is of class $C^{1,1}$, $f \in W^{1,p}(\mathbb{R}^N)$, $g \in W^{2,p}(\mathbb{R}^N)$, and $p \geq 2$. Then the map $\theta \mapsto \overline{u}(\theta) := u(\Omega_\theta)\circ(\mathrm{Id}+\theta) \in V(\Omega_0)$ is Fréchet differentiable in a neighbourhood of $\theta = 0$, and its directional derivative $L := \langle \overline{u}'(0), \theta\rangle$ is the unique solution in $V(\Omega_0)$ of the linearized state equation derived in [25, Prop. 10].*

The proof is given in detail in [25, §2.1] and we do not reproduce it here. We only retain that $\theta \mapsto J(\Omega_\theta)$ is Fréchet differentiable at 0, which is the key fact required by the Céa method described below.

5.2 Volume form of the shape gradient

We are now in a position to state and prove the main result.

Theorem 5.2 (Shape derivative of the compliance). *Under the assumptions of Proposition 5.1, the compliance J is shape differentiable at Ω_0 and, for every $\theta \in W^{1,\infty}(\mathbb{R}^N, \mathbb{R}^N)$ with $\theta = 0$ on $\overline{\Gamma_D} \cup \overline{\Gamma_N}$,*

$$J'(\Omega_0)(\theta) = \frac{1}{p-1}\int_{\Omega_0} \mathrm{div}\big[(p\,fu - |\nabla u|^p)\,\theta\big]\,dx. \tag{5.1}$$

If in addition Ω_0 is of class C^2, then

$$\boxed{J'(\Omega_0)(\theta) \;=\; \frac{1}{p-1}\int_\Gamma (p\,fu - |\nabla u|^p)\;\theta\cdot n\,ds\,.} \tag{5.2}$$

Proof (sketch). The proof applies Céa's Lagrangian method [1, 5, 16]. At the saddle point (u,q) of the Lagrangian (4.1), the chain rule gives $J'(\Omega_0)(\theta) = \partial_\Omega \mathcal{L}(\Omega_0, u, q)(\theta)$. Using that θ vanishes on $\Gamma_D \cup \Gamma_N$ and applying the shape-derivative formulas for volume and surface integrals (Lemmas 2.2, 2.3),

$$J'(\Omega_0)(\theta) = \int_\Gamma \big[fu - |\nabla u|^{p-2}\nabla u\cdot\nabla q + fq\big](\theta\cdot n)\,ds.$$

Substituting the self-adjoint identity $q = u/(p-1)$ from Theorem 4.3 yields (5.2). Equation (5.1) follows by the divergence theorem. A complete derivation is provided in Appendix A of the Supplementary Material. □

Corollary 5.3 (Recovery of the linear case)**.** *For $p = 2$, formula (5.2) reduces to*

$$J'(\Omega_0)(\theta) = \int_\Gamma (2fu - |\nabla u|^2)\theta \cdot n\, ds,$$

which is the classical shape gradient of the linear compliance, see, e.g. [1, Theorem 6.21].

Corollary 5.4 (Hadamard structure)**.** *The shape gradient (5.2) depends on θ only through its normal trace $\theta \cdot n$ on Γ, in agreement with the Hadamard structure theorem [16, 23].*

Remark 5.5 (Shape gradient density and steepest descent)**.** *Equation (5.2) reads $J'(\Omega_0)(\theta) = \int_\Gamma G\,\theta \cdot n\, ds$ with density $G(x) := (p-1)^{-1}(pfu - |\nabla u|^p)$. The $L^2(\Gamma)$-steepest descent direction is $\theta \cdot n = -G$. When $f \equiv 0$ in Ω, $G = -|\nabla u|^p/(p-1) \le 0$ so enlarging Ω decreases the compliance.*

6 Existence of optimal shapes

Without regularity restrictions, minimizing sequences may develop microstructure [1, 16]. Following Murat–Simon [20], we restrict the admissible class to shapes uniformly close to Ω_0 in the diffeomorphism metric.

Theorem 6.1 (Existence of optimal shapes)**.** *Let $R > 0$ and $V_0 > 0$ be such that $\mathcal{U}^R_{\mathrm{ad}}$ defined in (3.6) is non-empty. Then the optimization problem (3.6) admits at least one solution $\Omega^\star \in \mathcal{U}^R_{\mathrm{ad}}$.*

Proof (sketch). Step 1. The minimizing transformations $T_n = \mathrm{Id} + \theta_n$ are bounded in $W^{1,\infty}(\mathbb{R}^N, \mathbb{R}^N)$; Banach–Alaoglu and Arzelà–Ascoli extract a subsequence converging weakly-$*$ to $\theta^\star \in W^{1,\infty}$ and strongly in $C^0(\overline{\Omega_0})$, with limit $\Omega^\star = T^\star(\Omega_0)$ such that $d(\Omega^\star, \Omega_0) \le R$. *Step 2.* The volume map being continuous on $\mathcal{C}(\Omega_0)$ (Lemma 2.1), $|\Omega^\star| = V_0$. *Step 3.* The pulled-back states $\overline{u}_n = u_n \circ T_n$ are uniformly bounded in $V(\Omega_0)$; weak compactness and lower semicontinuity of the p-Dirichlet energy, combined with the strong C^0 convergence of T_n, yield $\overline{u}_n \rightharpoonup \overline{u}^\star$ and $\overline{u}^\star = u(\Omega^\star) \circ T^\star$. *Step 4.* A Γ-convergence argument ([16, Th. 13.1.4]) applied to the convex integrand $A_n(y,\xi) = |(\nabla T_n)^{-\top}\xi|^p|\det \nabla T_n|$ gives $J(\Omega^\star) \le \liminf_n J(\Omega_n) = \inf_{\mathcal{U}^R_{\mathrm{ad}}} J$. The full proof is in Appendix B of the Supplementary Material. □

Remark 6.2. *The volume constraint is essential: without it the infimum is $-\infty$ or attained at a degenerate design. It is enforced in Section 7 by Lagrange-multiplier projection.*

7 Numerical algorithm

The algorithm exploits Theorems 4.3 and 5.2.

7.1 Steepest descent direction

By Theorem 5.2, $J'(\Omega)(\theta) = \int_\Gamma G\,\theta \cdot n\, ds$ with $G := (pfu - |\nabla u|^p)/(p-1)$. The $L^2(\Gamma)$-steepest direction $\theta \cdot n = -G$ produces unstable boundary motions; the standard remedy [1, 21] is to find $V \in H^1(\Omega; \mathbb{R}^N)$ such that

$$\int_\Omega (\alpha^2 \nabla V : \nabla W + V \cdot W)\, dx = -\int_\Gamma G\,(W \cdot n)\, ds, \qquad \forall W \in H^1(\Omega; \mathbb{R}^N), \tag{7.1}$$

with the homogeneous Dirichlet condition $V = 0$ on $\Gamma_D \cup \Gamma_N$ to enforce that these portions of the boundary do not move. Here $\alpha > 0$ is a regularization length.

Lemma 7.1. *The vector field V defined by (7.1) is a descent direction for J, in the sense that $J'(\Omega)(V) = -\|V\|^2_{H^1_\alpha} < 0$ unless $G \equiv 0$ on Γ (a stationarity condition).*

Proof. Take $W = V$ in (7.1): $\|V\|^2_{H^1_\alpha} = -\int_\Gamma G(V \cdot n)\, ds = -J'(\Omega)(V)$. □

7.2 Volume constraint

We use the augmented density $G_\lambda := G + \lambda$ with Uzawa update $\lambda^{(k+1)} = \lambda^{(k)} + \beta(|\Omega^{(k)}| - V_0)$, $\beta > 0$, converging in practice for moderate β.

7.3 Algorithm

Algorithm 1 Adjoint-free shape gradient descent for p-Laplacian compliance

1: **Input:** initial domain $\Omega^{(0)}$, exponent p, loads f, g, target volume V_0, descent step $\tau_0 > 0$, regularization $\alpha > 0$, tolerances $\varepsilon_J, \varepsilon_g$.
2: Set $\lambda^{(0)} \leftarrow 0$, $k \leftarrow 0$.
3: **repeat**
4: Solve the p-Laplacian state (3.1) on $\Omega^{(k)}$ to obtain $u^{(k)}$ ▹ e.g. Newton or successive substitution
5: **[Self-adjoint shortcut]** Set $q^{(k)} \leftarrow u^{(k)}/(p-1)$ (Theorem 4.3)
6: Compute the gradient density on Γ:

$$G^{(k)}(x) \leftarrow \frac{p\, f(x)\, u^{(k)}(x) - |\nabla u^{(k)}(x)|^p}{p-1} + \lambda^{(k)}.$$

7: Solve the regularization problem (7.1) for $V^{(k)} \in H^1(\Omega^{(k)}; \mathbb{R}^N)$ with right-hand side $-G^{(k)} n$.
8: Line search: choose $\tau_k \in (0, \tau_{\max}]$ such that $J(\Omega^{(k)} + \tau_k V^{(k)}) < J(\Omega^{(k)})$.
9: Update domain: $\Omega^{(k+1)} \leftarrow (\mathrm{Id} + \tau_k V^{(k)})(\Omega^{(k)})$.
10: Update Lagrange multiplier: $\lambda^{(k+1)} \leftarrow \lambda^{(k)} + \beta(|\Omega^{(k+1)}| - V_0)$.
11: $k \leftarrow k + 1$.
12: **until** $|J(\Omega^{(k)}) - J(\Omega^{(k-1)})| < \varepsilon_J$ **and** $\|G^{(k)}\|_{L^2(\Gamma)} < \varepsilon_g$
13: **Output:** $\Omega^{(k)}$ and $u^{(k)}$.

7.4 Discretization

We discretize $\Omega^{(k)}$ by a triangular finite-element mesh $\mathcal{T}_h$ and use $\mathbb{P}^1$ Lagrange elements for $u^{(k)}$ and $V^{(k)}$. The domain update in line 9 is performed by displacing the mesh nodes: $x_i^{(k+1)} = x_i^{(k)} + \tau_k V^{(k)}(x_i^{(k)})$. When mesh distortion exceeds a quality threshold, the mesh is regenerated. The p-Laplacian state is solved by a damped Newton method initialized from the previous iteration:

$$\int_{\Omega^{(k)}} A(\nabla u_h^{(j)}) \nabla \delta u \cdot \nabla v_h = \int_{\Omega^{(k)}} f v_h + \int_{(\Gamma_N)_h} g v_h - \int_{\Omega^{(k)}} |\nabla u_h^{(j)}|^{p-2} \nabla u_h^{(j)} \cdot \nabla v_h,$$

with $A(\xi) := |\xi|^{p-2} I + (p-2)|\xi|^{p-4} \xi \otimes \xi$ being the Jacobian of $\xi \mapsto |\xi|^{p-2}\xi$.

7.5 Convergence analysis

In the spirit of [2, 3], we prove that the iterates of Algorithm 1 admit a subsequence converging to a critical point of the constrained problem. The step size $\tau_k > 0$ is chosen by an Armijo line-search,

$$J(\Omega^{(k+1)}) \;\le\; J(\Omega^{(k)}) + \sigma\, \tau_k\, J'(\Omega^{(k)})(V^{(k)}), \quad 0 < \sigma < 1, \tag{7.2}$$

with $\Omega^{(k+1)} = (\mathrm{Id} + \tau_k V^{(k)})(\Omega^{(k)})$. A curvature lower bound $\tau_k \geq \tau_{\min} > 0$ (enforced by the limit $\tau_k \geq d_{\max} \cdot 2^{-10}/\|V^{(k)}\|_{L^\infty}$ on the backtracks) prevents asymptotic step starvation.

Theorem 7.2 (Subsequential convergence to a critical point)**.** *Under the assumptions of Theorem 6.1, suppose moreover that the line-search rule (7.2) is satisfied at every iteration with $\tau_k \geq \tau_{\min} > 0$. Then:*

(i) the sequence $(J(\Omega^{(k)}))$ is monotonically decreasing and converges to a finite limit $J^\star \in \mathbb{R}$;

(ii) $\sum_{k=0}^{\infty} \|V^{(k)}\|^2_{H^1_\alpha} < +\infty$, and in particular $\|V^{(k)}\|_{H^1_\alpha} \to 0$ as $k \to \infty$;

(iii) there exists a subsequence $(\Omega^{(k_j)})$ converging in the pseudo-distance (2.4) to a domain $\Omega^\star \in \mathcal{U}^R_{\mathrm{ad}}$ that is a first-order critical point *of the volume-constrained shape optimization problem (3.6), i.e. there exists $\lambda^\star \in \mathbb{R}$ such that*

$$J'(\Omega^\star)(\theta) + \lambda^\star \int_{\Gamma^\star} \theta \cdot n \, ds \;=\; 0, \qquad \forall\, \theta \in W^{1,\infty}(\mathbb{R}^N, \mathbb{R}^N),\ \theta = 0 \text{ on } \overline{\Gamma_D \cup \Gamma_N}. \tag{7.3}$$

Proof (sketch). The Armijo rule together with $J'(\Omega^{(k)})(V^{(k)}) = -\|V^{(k)}\|^2_{H^1_\alpha}$ and $J \geq 0$ yields $\sum_k \|V^{(k)}\|^2_{H^1_\alpha} < \infty$, hence (i)–(ii). Murat–Simon compactness extracts a subsequence $\Omega^{(k_j)} \to \Omega^\star$ with $u^{(k_j)} \rightharpoonup u^\star$ in $W^{1,p}$ and $G^{(k_j)} \to G^\star$ in $L^{p'/p}(\Gamma^\star)$. Passing to the limit in (7.1) and using $\|V^{(k_j)}\| \to 0$ yields the critical-point identity (7.3) via Theorem 5.2. The full proof is in Appendix C of the Supplementary Material. ◻

Remark 7.3 (Strength and limits)**.** *Theorem 7.2 forces $\|V^{(k)}\| \to 0$ but provides no rate, and does not rule out saddle-point limits. Sharper results would require Łojasiewicz-type inequalities [9], not yet available for $p \neq 2$.*

8 Numerical experiments

8.1 Test case and implementation

Algorithm 1 is illustrated on a two-dimensional cantilever. The hold-all is the rectangle $D = (0, 2) \times (0, 1)$ with boundary partition

$$\Gamma_D = \{0\} \times [0, 1], \quad \Gamma_N = \{2\} \times [\tfrac{1}{2} - \delta, \tfrac{1}{2} + \delta], \quad \Gamma = \partial D \setminus (\Gamma_D \cup \Gamma_N), \tag{8.1}$$

$\delta = 0.10$, $f \equiv 0$, $g \equiv -1$ on Γ_N, target volume $V_0 = 2$. The initial domain is $\Omega_0 = D$ (Figure 1).

State and regularisation are discretised by piecewise-linear $\mathbb{P}^1$ elements on a structured triangulation. The p-Laplacian is solved by damped Newton warm-started with the linear Laplace solution; the self-adjoint identity (Theorem 4.3) makes the adjoint free. The descent direction (7.1) decouples into two scalar elliptic problems with the same matrix and right-hand sides $-Gn_x$, $-Gn_y$. The mesh is moved by $x \mapsto x + \tau V(x)$ with $\tau \leq d_{\max}/\|V\|_{L^\infty}$, $d_{\max} = 0.2h$; the step is halved until `checkmovemesh` succeeds.

Volume-preserving projection. We replace the Uzawa rule by an exact H^1_α-orthogonal projection. Let $V^{(0)}$ solve (7.1) with right-hand side $-Gn$ and $V^{(1)}$ with right-hand side $-n$; then $V := V^{(0)} - \mu V^{(1)}$ with $\mu = \int_\Gamma V^{(0)} \cdot n \, ds \,/ \int_\Gamma V^{(1)} \cdot n \, ds$ satisfies $\int_\Gamma V \cdot n \, ds = 0$. The numerical volume drift is bounded by 7×10^{-4} (0.04% of V_0) over 60–70 iterations (Figure 4).

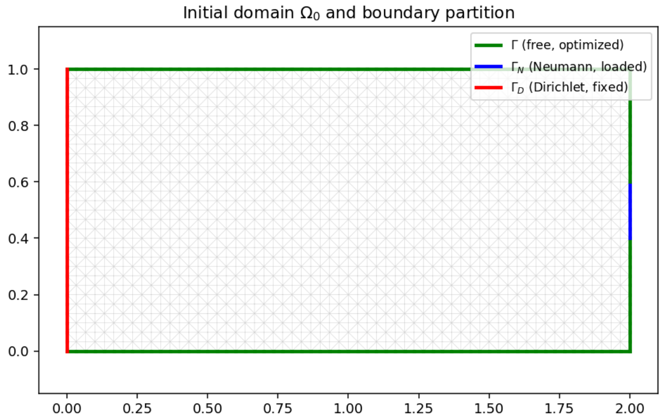

Figure 1. Initial domain $\Omega_0 = (0, 2) \times (0, 1)$ and partition (8.1): Γ_D (red), Γ_N (blue), Γ (green). Mesh: 1 891 nodes, 3 600 triangles.

8.2 Verification of the shape gradient by finite differences

We verify formula (5.2) by comparing the analytic shape derivative against a finite-difference secant. The test direction $V \in W^{1,\infty}(\mathbb{R}^N, \mathbb{R}^N)$ is the H^1-regularization of $-G\,n$ on Ω_0, normalized to $\|V\|_{L^\infty} = 1$. The analytic value $J'(\Omega_0)(V)$ is evaluated by exact $\mathbb{P}^1 \times \mathbb{P}^1$ quadrature on Γ; the finite-difference secant $J'_{\mathrm{FD}}(t) := [J((\mathrm{Id} + tV)\Omega_0) - J(\Omega_0)]/t$ converges to it at first order in t. Table 1 reports the relative error for $p \in \{1.5, 2, 3, 4\}$ and decreasing step sizes; linear decay in t validates the formula. The small-t floor reflects the $\mathbb{P}^1$ discretization error of the state, not of the shape-derivative formula itself; it is largest for $p = 1.5$ because the singular operator near $|\nabla u| = 0$ reduces local accuracy. Employing higher-order elements such as $\mathbb{P}^2$ Lagrange elements would raise the formal approximation order of the state and of the boundary quadrature of $|\nabla u|^p$, and is therefore expected to lower the stagnation floor observed at $t = 10^{-4}$ for $p = 1.5$; the improvement should however be only partial in the singular regime, since the exact state has limited Sobolev regularity near the degeneracy set $\{\nabla u = 0\}$ and the finite-element convergence rate for the p-Laplacian is capped by this regularity rather than by the polynomial degree, so that $\mathbb{P}^2$ elements mitigate, but do not eliminate, the residual plateau; a quantitative comparison is left for future work.

Table 1. Finite-difference verification of Theorem 5.2. The relative error $|J'_{\mathrm{FD}}(t) - J'(\Omega_0)(V)|/|J'(\Omega_0)(V)|$ decreases with t, matching first-order accuracy.

p	$J'(\Omega_0)(V)$	$t = 10^{-2}$	$t = 10^{-3}$	$t = 5{\cdot}10^{-4}$	$t = 10^{-4}$
1.5	$-6.258{\cdot}10^{-2}$	$1.68{\cdot}10^{-1}$	$9.30{\cdot}10^{-2}$	$8.86{\cdot}10^{-2}$	$8.51{\cdot}10^{-2}$
2.0	$-8.723{\cdot}10^{-2}$	$7.45{\cdot}10^{-2}$	$2.53{\cdot}10^{-2}$	$2.24{\cdot}10^{-2}$	$2.01{\cdot}10^{-2}$
3.0	$-9.599{\cdot}10^{-2}$	$4.29{\cdot}10^{-2}$	$9.10{\cdot}10^{-3}$	$7.16{\cdot}10^{-3}$	$5.60{\cdot}10^{-3}$
4.0	$-8.677{\cdot}10^{-2}$	$3.87{\cdot}10^{-2}$	$8.74{\cdot}10^{-3}$	$7.02{\cdot}10^{-3}$	$5.63{\cdot}10^{-3}$

Last four columns: relative error of $J'_{\mathrm{FD}}(t)$.

8.3 Optimal shapes

Algorithm 1 is run for $p \in \{1.5, 2, 3, 4\}$ with $\alpha = 0.10$, $d_{\max} = 0.2h$, $h = 1/30$, $V_0 = 2$. Convergence is reached in 60–70 iterations ($\sim$ 30 s per value on a standard laptop). Figure 2 shows the optimal domains $\Omega_p^\star$; Table 2 reports final compliances and reductions.

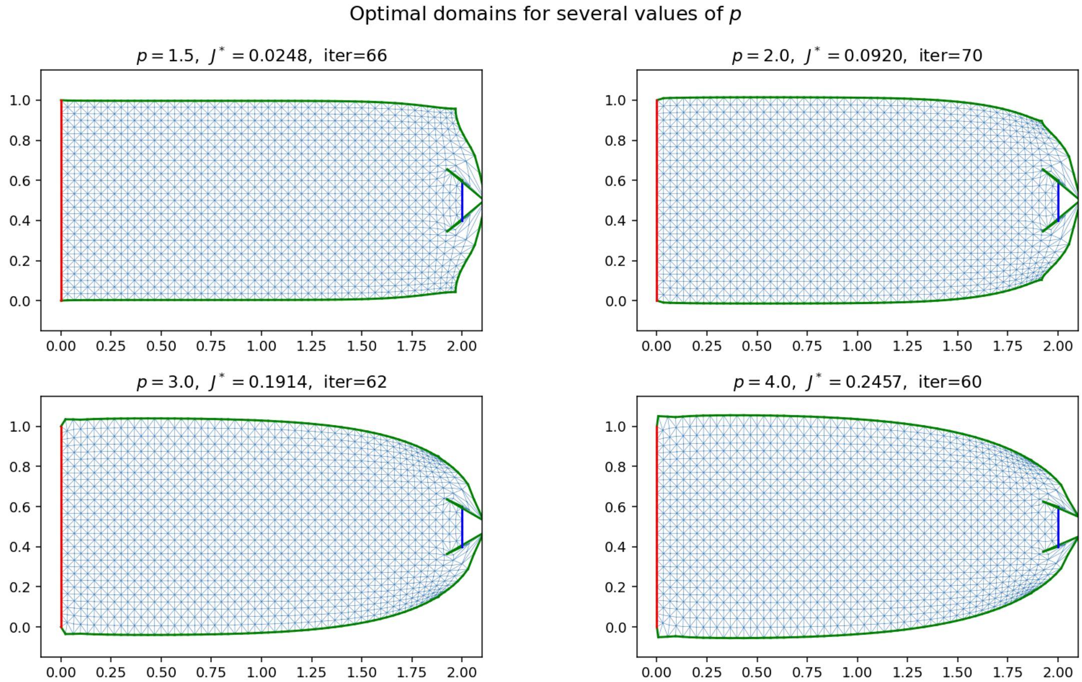

Figure 2. Optimal domains $\Omega_p^\star$ for $p \in \{1.5, 2, 3, 4\}$. Free boundary Γ (green), loaded Γ_N (blue), clamped Γ_D (red). Volume conserved to 0.04%. Larger p gives rounded drop-shaped designs; $p = 1.5$ concentrates material along the load path.

Table 2. Compliance reduction for the four values of p. The initial domain is the rectangle $\Omega_0 = (0, 2)\times(0, 1)$, common to all runs.

p	iterations	$J(\Omega_0)$	$J(\Omega_p^\star)$	reduction
1.5	66	0.02783	0.02482	**10.83**%
2.0	70	0.09577	0.09201	3.92%
3.0	62	0.19513	0.19137	1.93%
4.0	60	0.24922	0.24573	1.40%

8.4 Convergence histories, volume conservation, state

Compliance histories $k \mapsto J(\Omega_p^{(k)})$ (Figure 3) are monotonically decreasing. Relative reductions depend strongly on p: $> 10\%$ for $p = 1.5$, $< 1.5\%$ for $p = 4$ — the rectangle is closer to the optimum for super-quadratic membranes. Volume drift (Figure 4) is bounded by 7×10^{-4} (0.04% of V_0), at the second-order error level of the H^1 projection. The state u on each $\Omega_p^\star$ (Figure 5) has amplitude $\|u\|_{L^\infty}$ that grows with p, a feature of the super-linear p-Laplacian at large gradient magnitudes [10, 17].

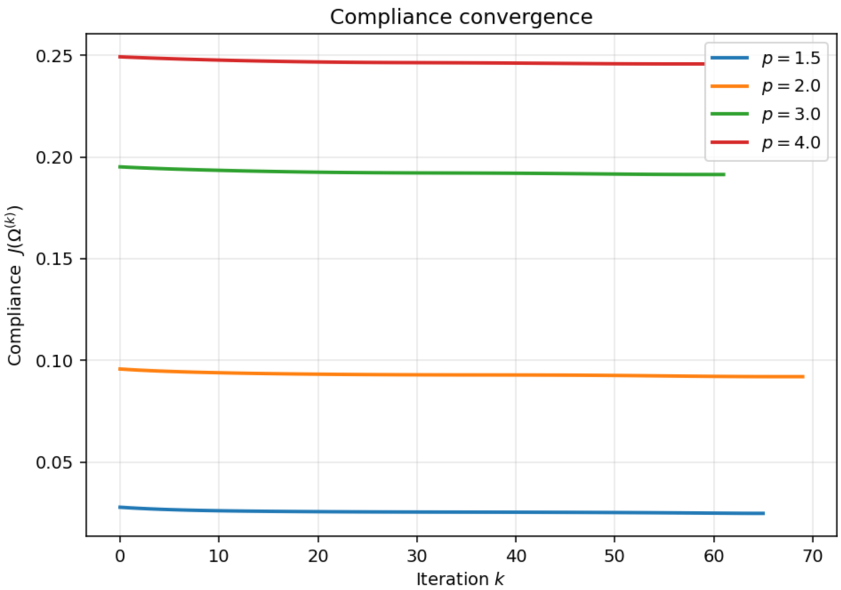

Figure 3. Compliance histories $k \mapsto J(\Omega_p^{(k)})$, monotonically decreasing.

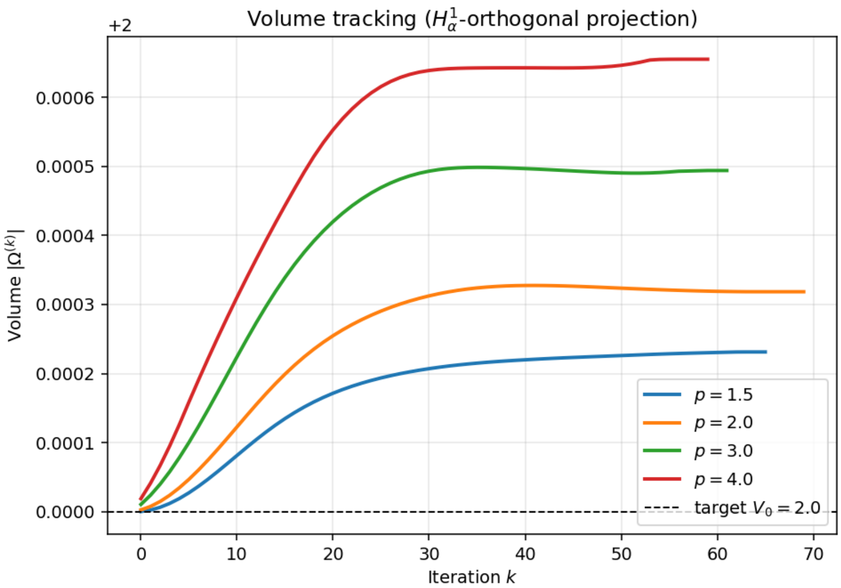

Figure 4. Volume tracking. Drift stays within $\pm 7 \times 10^{-4}$ of $V_0 = 2$ for all p.

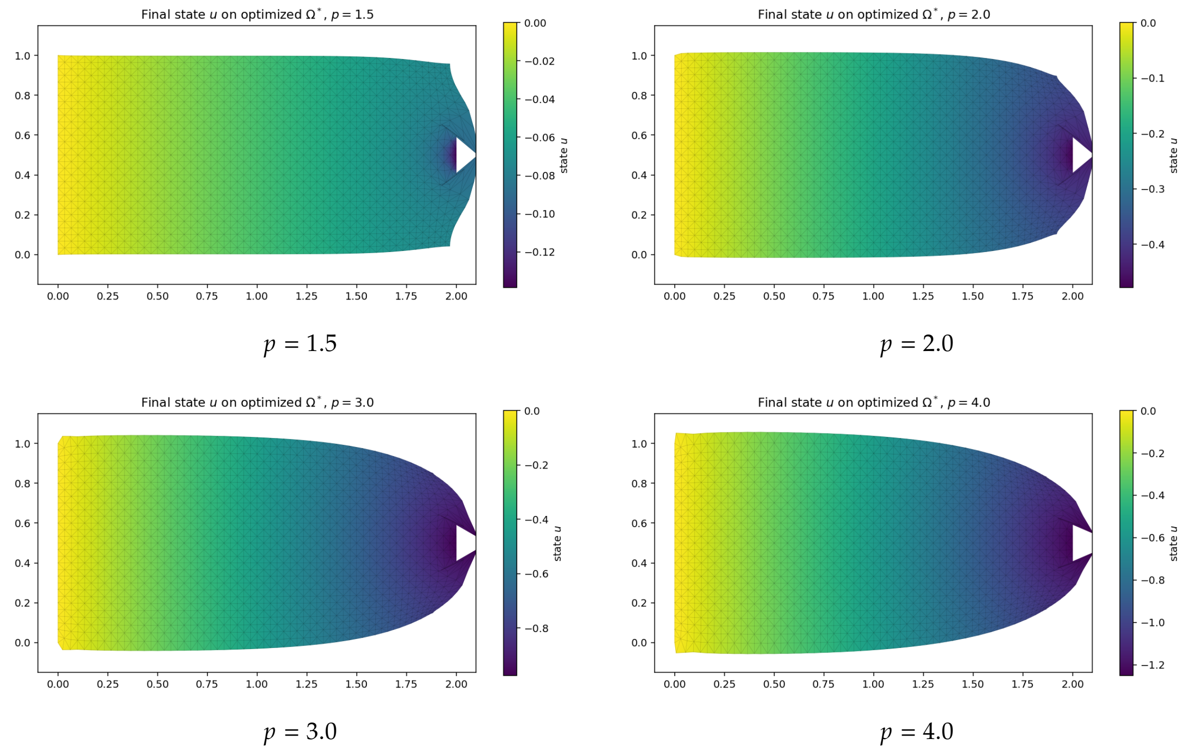

$p = 1.5$ $p = 2.0$ $p = 3.0$ $p = 4.0$

Figure 5. Final state u on $\Omega_p^\star$ for each p.

8.5 Mesh refinement study

We run the cantilever benchmark for $p = 2$ on structured meshes with $h \in \{1/15, 1/30, 1/45\}$. Table 3 reports the converged compliance $J_h^\star$, iteration counts and CPU times. The compliance exhibits super-linear convergence with measured rate ≈ 3.6, consistent with the $O(h^2)$ accuracy of $\mathbb{P}^1$ elements on rectangular domains. Figure 6 shows the error in log-log scale.

Table 3. Mesh refinement (cantilever, $p = 2$). Reference $J^\star_{h_{\min}} = 0.09316$.

N_x	N_y	h	iterations	$J_h^\star$	CPU (s)
30	15	0.0667	50	0.0895	1.3
60	30	0.0333	50	0.0929	4.6
90	45	0.0222	50	0.0932	10.8

Observed rate (first two levels): 3.6.

8.6 Three test cases

To demonstrate robustness across geometries, we run the algorithm on three classical benchmarks for $p \in \{1.5, 2, 3\}$: (T1) **Cantilever** (above); (T2) **MBB beam**: rectangle $(0, 4) \times (0, 1)$, two narrow Dirichlet supports at the bottom corners, downward unit load on a portion of the top-left edge [4]; (T3) **Bridge / short column**: rectangle $(0, 2) \times (0, 1)$, two narrow Dirichlet feet at the bottom corners, distributed downward load on the top edge.

Results are summarised in Table 4; optimal shapes are shown in Figures 7 and 8.

Relative compliance reductions reach 51.8% on the MBB beam at $p = 1.5$. The qualitative trend—more diffuse, rounded designs at large p and sharper, truss-like designs at $p < 2$—is consistent across all cases.

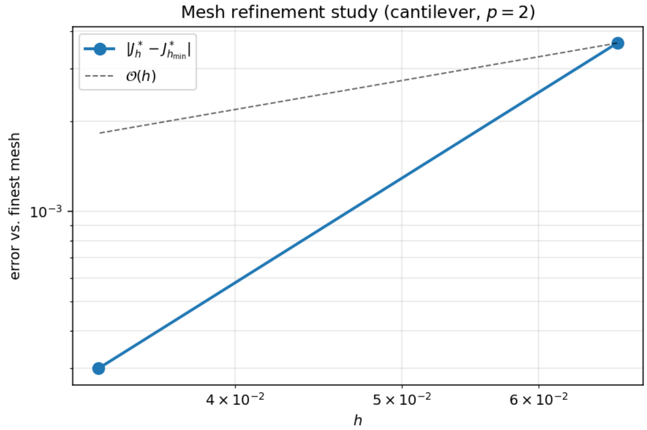

Figure 6. Mesh refinement (cantilever, $p = 2$): error $|J_h^\star - J_{h_{\min}}^\star|$ vs. h, log-log scale.

Table 4. Compliance reduction for three test cases, $p \in \{1.5, 2, 3\}$.

test case	p	iterations	$J(\Omega_0)$	$J(\Omega_p^\star)$	reduction
cantilever	1.5	50	0.0278	0.0254	8.7%
	2.0	50	0.0958	0.0929	3.0%
	3.0	50	0.1951	0.1921	1.6%
MBB beam	1.5	45	0.0357	0.0172	**51.8%**
	2.0	46	0.0852	0.0530	**37.7%**
	3.0	40	0.1393	0.1063	**23.7%**
bridge	1.5	50	10.5704	5.4190	**48.7%**
	2.0	50	3.8972	3.2366	**17.0%**
	3.0	50	2.8273	2.6546	6.1%

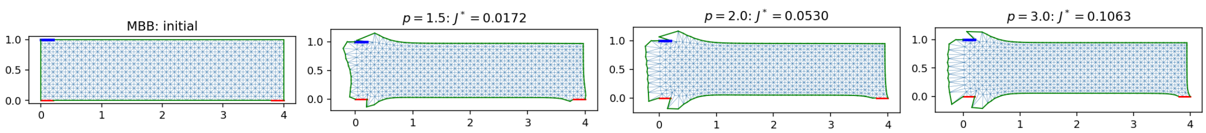

Figure 7. MBB beam: initial domain (left) and optimal shapes for $p \in \{1.5, 2, 3\}$ (next three panels). Compliance reductions exceed 50% for $p = 1.5$.

Latin American Journal of Mathematics, Vol. 5, No. 1, 2026, pp. 69–87

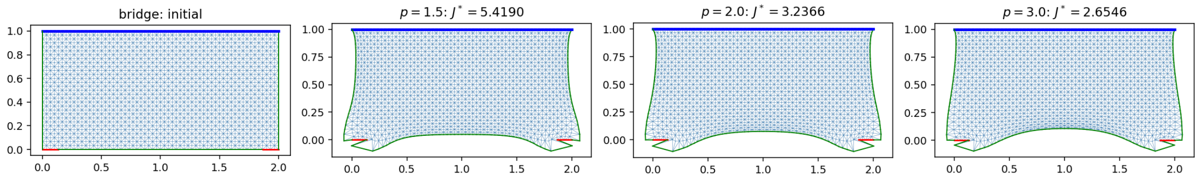

Figure 8. Bridge / short column. Two clamped feet at the bottom corners and a distributed load on the top edge produce an arch profile; the arch sharpens as p decreases.

8.7 CPU comparison: shortcut vs. full adjoint solve

We implement two variants of the algorithm differing only in the adjoint state: (i) *shortcut* $q = u/(p-1)$ (zero extra PDE solves); (ii) *full adjoint*, solving (4.3) by a sparse direct solver on the assembled Jacobian B_u. Both produce identical iterates to floating-point precision, a numerical confirmation of Theorem 4.3. Table 5 reports cumulative wall-clock times over 50 iterations of the cantilever for $p \in \{1.5, 2, 3\}$.

Table 5. CPU comparison: shortcut vs. full adjoint. t_{adj} is the adjoint cost; speedup is the total-time ratio.

p	method	iter	$J^\star$	total CPU (s)	t_{adj} (s)	speedup
1.5	shortcut	50	0.02525	34.59	0.0003	—
	full adjoint	50	0.02525	36.85	1.110	1.07×
2.0	shortcut	50	0.09265	4.57	0.0003	—
	full adjoint	50	0.09265	5.74	0.972	1.25×
3.0	shortcut	50	0.19164	35.09	0.0003	—
	full adjoint	50	0.19164	36.17	1.176	1.03×

The agreement $J^\star_{\text{short}} = J^\star_{\text{full}}$ to all reported digits validates Theorem 4.3. The speedup is largest for $p = 2$ (about 25%), where the state solve is fast (linear) and the adjoint dominates the per-iteration cost. For $p \neq 2$ the Newton iteration dominates, giving a modest speedup of 3–7%. Beyond raw speed, the shortcut avoids assembling the degenerate $|\nabla u|^{p-2}$-weighted Jacobian, saves memory, and is a one-line replacement in any existing solver.

8.8 Implementation

A FreeFem++ [15] implementation (Appendix D of the Supplementary Material) and a Python implementation (numpy/scipy/matplotlib) reproduce all experiments. The self-adjoint shortcut $q = u/(p-1)$ appears as a one-line replacement of the adjoint solve.

9 Conclusion and perspectives

We obtained four main results on shape optimization of the p-Laplacian compliance.

Structural identities. (i) The optimal-control system is self-adjoint up to $1/(p-1)$, so $q = u/(p-1)$ (Theorem 4.3); the functional setting is $V(\Omega)$ for $p \geq 2$ and the weighted Sobolev space $H^1_\omega(\Omega; \Gamma_D)$ with $\omega = |\nabla u|^{p-2}$ for $1 < p < 2$ (Proposition 4.5). (ii) The shape gradient admits the boundary expression (5.2) involving only the primal state (Theorem 5.2).

Algorithmic outcome. (iii) The algorithm needs one nonlinear PDE solve per iteration instead of two; speedup is 3–25%, peaking at $p = 2$. (iv) Subsequential convergence to a first-order critical point holds (Theorem 7.2) under an Armijo line-search.

Numerical validation. Finite differences (Table 1) confirm first-order convergence; mesh refinement (Table 3) gives a rate ≈ 3.6. On three benchmarks the compliance drops by up to 51.8% (MBB, $p = 1.5$), volume conserved to 0.04%. The CPU comparison (Table 5) confirms identical iterates between shortcut and full-adjoint methods.

Perspectives. The doubly-nonlinear (p, q)-Laplacian, the $p(x)$-Laplacian for electrorheological materials and image processing [18], for which nonsmooth descent strategies of the type developed in [13] appear well suited, topological derivatives, and robust optimization under uncertainty on f, g are natural extensions. Combining the shortcut with level-set mesh evolution [2, 7] would allow topological changes.

Acknowledgements

The author thanks colleagues at the Department of Mathematics, University Mohammed I, Oujda, for valuable discussions on earlier versions of this manuscript.

Funding

This research did not receive any specific grant from funding agencies in the public, commercial, or not-for-profit sectors.

Declaration of competing interests

The author declares that he has no known competing financial interests or personal relationships that could have appeared to influence the work reported in this paper.

Data availability

The Python and FreeFem++ codes that support the findings of this study are openly available as supplementary material accompanying this submission.

References

[1] G. Allaire, *Conception optimale de structures*, Mathématiques & Applications, vol. 58, Springer, Berlin, 2007, DOI 10.1007/978-3-540-36856-4.

[2] G. Allaire, C. Dapogny, and F. Jouve, *Shape and topology optimization*, Geometric Partial Differential Equations, Part II (A. Bonito and R. H. Nochetto, eds.), Handbook of Numerical Analysis, vol. 22, Elsevier, Amsterdam, 2021, DOI 10.1016/bs.hna.2020.10.004, pp. 1–132.

[3] G. Allaire, F. Jouve, and A.-M. Toader, *A level-set method for shape optimization*, C. R. Math. Acad. Sci. Paris **334** (2002), no. 12, 1125–1130, DOI 10.1016/S1631-073X(02)02412-3.

[4] M. P. Bendsøe and O. Sigmund, *Topology optimization: Theory, methods, and applications*, Springer, Berlin, 2003, DOI 10.1007/978-3-662-05086-6.

[5] J. Céa, *Conception optimale ou identification de formes: calcul rapide de la dérivée directionnelle de la fonction coût*, RAIRO Modél. Math. Anal. Numér. **20** (1986), no. 3, 371–402, DOI 10.1051/m2an/1986200303711.

[6] D. Cruz-Uribe, K. Moen, and S. Rodney, *Matrix A_p weights, degenerate Sobolev spaces, and mappings of finite distortion*, J. Geom. Anal. **26** (2016), no. 4, 2797–2830, DOI 10.1007/s12220-015-9649-8.

[7] C. Dapogny and F. Feppon, *Shape optimization using a level set based mesh evolution method: an overview and tutorial*, C. R. Math. Acad. Sci. Paris **361** (2023), 1267–1332, DOI 10.5802/crmath.498.

[8] K. Deckelnick, P. J. Herbert, and M. Hinze, *A novel $W^{1,\infty}$ approach to shape optimisation with Lipschitz domains*, ESAIM Control Optim. Calc. Var. **28** (2022), 1–29, DOI 10.1051/cocv/2021108.

[9] K. Deckelnick, P. J. Herbert, and M. Hinze, *Convergence of a steepest descent algorithm in shape optimisation using $W^{1,\infty}$ functions*, ESAIM Math. Model. Numer. Anal. **59** (2025), no. 3, 1505–1529, DOI 10.1051/m2an/2025033.

[10] E. DiBenedetto, *Degenerate parabolic equations*, Universitext, Springer, New York, 1993, DOI 10.1007/978-1-4612-0895-2.

[11] E. B. Fabes, C. E. Kenig, and R. P. Serapioni, *The local regularity of solutions of degenerate elliptic equations*, Comm. Partial Differential Equations **7** (1982), no. 1, 77–116, DOI 10.1080/03605308208820218.

[12] F. Feppon, G. Allaire, and C. Dapogny, *Null space gradient flows for constrained optimization with applications to shape optimization*, ESAIM Control Optim. Calc. Var. **26** (2020), Paper No. 90, DOI 10.1051/cocv/2020015.

[13] S. González-Andrade, *A preconditioned descent algorithm for variational inequalities of the second kind involving the p-Laplacian operator*, Comput. Optim. Appl. **66** (2017), no. 1, 123–162, DOI 10.1007/s10589-016-9861-x.

[14] J. Hadamard, *Mémoire sur le problème d'analyse relatif à l'équilibre des plaques élastiques encastrées*, Mémoires présentés par divers savants à l'Académie des Sciences **33** (1908), 1–128.

[15] F. Hecht, *New development in FreeFem++*, J. Numer. Math. **20** (2012), no. 3-4, 251–265, DOI 10.1515/jnum-2012-0013.

[16] A. Henrot and M. Pierre, *Variation et optimisation de formes: Une analyse géométrique*, Mathématiques & Applications, vol. 48, Springer, Berlin, 2005, DOI 10.1007/3-540-37689-5.

[17] P. Lindqvist, *Notes on the p-Laplace equation*, second ed., Report / University of Jyväskylä, Department of Mathematics and Statistics, vol. 161, University of Jyväskylä, Jyväskylä, 2017.

[18] M. Mihăilescu and V. Rădulescu, *On a nonhomogeneous quasilinear eigenvalue problem in Sobolev spaces with variable exponent*, Proc. Amer. Math. Soc. **135** (2007), no. 9, 2929–2937, DOI 10.1090/S0002-9939-07-08815-6.

[19] P. M. Müller, N. Kühl, M. Siebenborn, K. Deckelnick, M. Hinze, and T. Rung, *A novel p-harmonic descent approach applied to fluid dynamic shape optimization*, Struct. Multidiscip. Optim. **64** (2021), 3489–3503, DOI 10.1007/s00158-021-03030-x.

[20] F. Murat and J. Simon, *études de problèmes d'optimal design*, Optimization Techniques: Modeling and Optimization in the Service of Man, Part 2, Lecture Notes in Computer Science, vol. 41, Springer, Berlin, 1976, DOI 10.1007/3-540-07623-9_279, pp. 54–62.

[21] T. De Pauw and A. Henrot, *A finite element method for shape optimization with applications to free boundary problems*, Free Boundary Problems, International Series of Numerical Mathematics, Birkhäuser, Basel, 2005, pp. 141–150.

[22] O. Pironneau, *Optimal shape design for elliptic systems*, Springer Series in Computational Physics, Springer, New York, 1984, DOI 10.1007/978-3-642-87722-3.

[23] J. Sokolowski and J.-P. Zolésio, *Introduction to shape optimization: Shape sensitivity analysis*, Springer Series in Computational Mathematics, vol. 16, Springer, Berlin, 1992, DOI 10.1007/978-3-642-58106-9.

[24] H. Wyschka and M. Siebenborn, *Towards computing high-order p-harmonic descent directions and their limits in shape optimization*, Modeling, Simulation and Optimization of Fluid Dynamic Applications (A. Iske and T. Rung, eds.), Lecture Notes in Computational Science and Engineering, vol. 148, Springer, Cham, 2023, DOI 10.48550/arXiv.2208.06897, pp. 147–163.

[25] Y. Yousfi, I. Hadi, and A. Benbrik, *Optimal form for compliance of membrane boundary shift in nonlinear case*, Int. J. Math. Math. Sci. **2018** (2018), Art. ID 1689269, 9 pp., DOI 10.1155/2018/1689269.

[26] E. Zeidler, *Nonlinear functional analysis and its applications. II/B: Nonlinear monotone operators*, Springer, New York, 1990, DOI 10.1007/978-1-4612-0985-0.